Radio Metric Errors Due to Mismatch and Offset Between a DSN Antenna Beam and the Beam of a Troposphere Calibration Instrument

R. P. Linfield and J. Z. Wilcox
Tracking Systems and Applications Section

Two components of the error of a troposphere calibration measurement have been quantified by theoretical calculations. The first component is a beam mismatch error, which occurs when the calibration instrument senses a conical volume different from the cylindrical volume sampled by a DSN antenna. The second component is a beam offset error, which occurs if the calibration instrument is not mounted on the axis of the DSN antenna. These two error sources were calculated for both delay (e.g., VLBI) and delay rate (e.g., Doppler) measurements. The beam mismatch error for both delay and delay rate drops rapidly as the beamwidth of the troposphere calibration instrument (e.g., a water vapor radiometer or an infrared Fourier transform spectrometer) is reduced. At a 10-deg elevation angle, the instantaneous beam mismatch error is 1.0 mm for a 6-deg beamwidth and 0.09 mm for a 0.5-deg beam (these are the full angular widths of a circular beam with uniform gain out to a sharp cutoff). Time averaging for 60–100 sec will reduce these errors by factors of 1.2–2.2. At a 20-deg elevation angle, the lower limit for current Doppler observations, the beam-mismatch delay rate error is an Allan standard deviation over 100 sec of 1.1×10^{-14} with a 4-deg beam and 1.3×10^{-15} for a 0.5-deg beam.

A 50-m beam offset would result in a fairly modest (compared to other expected error sources) delay error (≤ 0.3 mm for 60-sec integrations at any elevation angle ≥ 6 deg). However, the same offset would cause a large error in delay rate measurements (e.g., an Allan standard deviation of 1.2×10^{-14} over 100 sec at a 20-deg elevation angle), which would dominate over other known error sources if the beamwidth is 2 deg or smaller. An on-axis location is essential for accurate troposphere calibration of delay rate measurements. A half-power beamwidth (for a beam with a tapered gain profile) of 1.2 deg or smaller is desired for calibration of all types of radio metrics. A water-vapor radiometer calibration beam of this size with very low sidelobes would require a clear aperture antenna with a diameter of at least 1.5 m if the primary water vapor sensing channel were in the 20–22 GHz range.

I. Introduction

A. Background

Spacecraft tracking with the DSN involves radio metric (delay or delay rate) measurements over the spacecraft–ground path, sometimes with similar measurements of natural radio sources for purposes of calibration. Any non-geometric delay or delay rate will (if not perfectly calibrated) degrade the accuracy of the tracking measurement. With the increase in the radio frequency used for spacecraft tracking from 2.3 GHz (past missions) to 8.4 GHz (current missions) to 32 GHz (future missions), the effect of charged particles along the spacecraft–ground path is becoming much less significant ($\tau_{ion} \propto \nu^{-2}$, where τ_{ion} is the delay due to charged particles and ν is the radio frequency of the link; the same proportionality holds for delay rates). The effect of the neutral (and nondispersive) troposphere is consequently becoming more dominant. For 8.4-GHz single-frequency observations, the contributions from charged particles and from the troposphere are comparable. For 32-GHz single-frequency tracking (future spacecraft missions) or for dual-frequency measurements (current very long baseline interferometry [VLBI] tracking), the troposphere will dominate over other media effects. The radio metric data themselves can be used to solve for the tropospheric delay. However, spatial and temporal irregularities in the troposphere limit the accuracy with which this process can be done.

A VLBI tracking demonstration on a natural source [1] showed that the tropospheric delay in the direction toward a spacecraft could be estimated to an accuracy of approximately 1 cm, giving an angular measurement accuracy of 1 nanoradian (nrad). *Troposphere calibration is essential in order to improve the accuracy of radio metric tracking beyond this capability.* For a goal of an order-of-magnitude improvement in VLBI tracking accuracy to 100 picoradians (prad), the contribution of the troposphere must be reduced to 1 mm, through a combination of calibration and parameter estimation.

Doppler (delay rate) spacecraft tracking measurements are used both for navigation and for gravitational wave searches. The troposphere calibration goals for future Doppler navigation using Ka-band (31–34 GHz) have not yet been completely specified. However, they are approximately 1×10^{-15} in an Allan standard deviation over 3000–10,000 sec.[1] For the Cassini Gravitational Wave Search experiment (the first one to use a Ka-band link), the *goals*

for troposphere calibration are Allan standard deviations of 4×10^{-16} at 1000 and 10,000 sec and 1.3×10^{-15} at 100 sec. The experiment *requirements* are a factor of 4 less stringent.[2] The goals for this experiment were chosen so that the contribution to the delay rate from the uncalibrated troposphere would not dominate the total error at any time scale.

In this article, the terms "delay" and "delay rate" refer to characteristics of the troposphere above a single DSN antenna. This is different than one common use of these terms in DSN spacecraft navigation, where "delay" and "delay rate" refer to the difference (or its time derivative) in arrival times at two DSN antennas (which are often widely spaced). For such station-differenced radio metric data types, the effects calculated here apply to both stations. For widely spaced stations (e.g., at different DSN sites), the delay and delay rate effects in this article should be added in quadrature.

B. Beam Mismatch and Offset

Several types of remote-sensing troposphere calibration systems have been constructed or proposed. These include water vapor radiometers (WVR's) [2], infrared Fourier transform spectrometers (FTS's) [3], and tracking of global positioning satellites (GPS's) [4]. For all these systems, the delay is measured (or inferred from thermal emission) over some volume of troposphere. This volume is approximately conical for techniques that measure emission (WVR, FTS) and cylindrical for techniques that measure delay or absorption (GPS). In both cases, the measured volume of troposphere will not match the volume sampled by a DSN antenna, which is cylindrical with a diameter equal to the DSN antenna diameter, axis centered on the antenna, and extending in the direction of the spacecraft or natural source that is being observed. This cylindrical shape results from the circular shape of the DSN aperture and the fact that the observed radio signal arises from a source on the sky that has a very small ($\ll$1-arcsec) angular extent. The volume mismatch can be broken down into two components: a mismatch in the beam shape and/or size (e.g., conical versus cylindrical) and a horizontal offset in the axes of the two instruments (resulting from the calibration instrument being mounted on the edge of the DSN antenna or off the antenna entirely). There are inhomogeneities in tropospheric refractivity, predominately due to variable water vapor density. As a result, both a beam mismatch and a beam offset would be expected to

cause significant errors. The purpose of this article is to quantify these errors.

Other error sources in the calibration process (e.g., the brightness temperature-to-path delay conversion for water-vapor radiometer measurements) will be important and are likely to be larger than the beam-mismatch and beam-offset errors in some cases. However, these error sources have been neglected in this article, so that the effect of the beam-mismatch and beam-offset errors can be more fully studied. In any case, these other (e.g., non-beam-related) error sources could potentially be reduced to very small levels by advanced instruments and data-processing techniques.

II. Definitions and Calculation Methods

A. Basic Definitions

The wet tropospheric delay $\tau_{DSN}(\vec{x}_{DSN}, t)$ sampled at time t by a DSN antenna of diameter d_{DSN} whose vertex is at position $\vec{x}_{DSN}$ and which is pointed at elevation angle θ_{DSN} and azimuth ϕ_{DSN} is

$$\tau_{DSN}(\vec{x}_{DSN}, t) = \frac{4}{\pi d_{DSN}^2 \sin \theta_{DSN}} \int_0^{d_{DSN}/2} R\, dR \int_0^{2\pi} d\omega$$

$$\times \int_{-R \cos \omega \cos \theta_{DSN}}^{h} dz\, \chi(\vec{x}_{DSN}$$

$$+ \vec{r}(\theta_{DSN}, \phi_{DSN}, R, \omega, z), t) \qquad (1)$$

where $\chi(\vec{x}, t)$ is the refractivity ($\chi \equiv n - 1$, where n is the index of refraction) associated with water vapor at position $\vec{x}$ and time t; $\vec{r}(\theta_{DSN}, \phi_{DSN}, R, \omega, z)$ is the position, relative to the antenna vertex, of a vector in direction $(\theta_{DSN}, \phi_{DSN})$ from polar coordinates (R, ω) on the antenna to height z (the antenna vertex is defined as lying at $z = 0$); and h is the height of the wet troposphere slab, above which χ is assumed to be negligible. The DSN aperture has been approximated by a flat disk. In Eq. (1), the delay has been integrated across the DSN aperture. The actual delay measured by a DSN antenna is derived from the phase of a spatially integrated complex signal. However, because the signal is coherent across the DSN aperture (i.e., the phase variations are <<1 rad), the phase of the integrated signal is equal to the integral of the phase across the aperture.

The wet troposphere delay $\tau_{cal}(\vec{x}_{cal}, t)$ measured at time t by a calibration instrument with a conical beam at location $\vec{x}_{cal}$ is

$$\tau_{cal}(\vec{x}_{cal}, t) = \frac{1}{\Omega} \int_0^{\psi/2} \sin u\, du \int_0^{2\pi} \frac{d\omega}{\sin \theta(u, \omega)}$$

$$\times \int_0^h dz\, \chi(\vec{x}_{cal} + \vec{r}(\theta, \phi, z), t) \qquad (2)$$

The calibration-beam cross section is assumed to be conical, with uniform gain out to a full angular width ψ. The correspondence between the full width of such a beam and the half-power beamwidth (HPBW) of a Gaussian beam profile is discussed in Section III.A. The beam solid angle Ω is $\Omega = 2\pi[1 - \cos(\psi/2)]$ and $\vec{r}(\theta, \phi, z)$ is the position at height z, relative to the calibration instrument, of a vector along elevation angle θ and azimuth ϕ.

In order for the difference between $\tau_{DSN}(\vec{x}_{DSN}, t)$ and $\tau_{cal}(\vec{x}_{cal}, t)$ to have zero mean, the axis of the calibration beam must be pointed at an elevation angle θ_{cal} that is higher than θ_{DSN}. There is a nonlinear gradient of air mass A with elevation angle θ across the calibration beam, so that the mean air mass corresponds to an elevation angle lower than θ_{cal}. [The air mass $A(\theta)$ is the tropospheric path length at elevation angle θ, normalized to the zenith path length, for a homogeneous troposphere. For the plane-parallel, zero-bending approximation used in these calculations, $A(\theta) = 1/\sin \theta$]. This effect has been previously noted [5]. For the circular calibration-beam cross section used here, θ_{cal} was calculated numerically. For the cases in this article, the largest value of $\theta_{cal} - \theta_{DSN}$ was 0.23 deg (for $\theta_{DSN} = 10$ deg and $\psi = 6$ deg). For a more typical case, the difference in elevation angles was much smaller (e.g., for $\theta_{DSN} = 20$ deg, $\psi = 1$ deg, $\theta_{cal} - \theta_{DSN} = 0.003$ deg).

The absolute value of the average instantaneous difference $\Delta \tau_{inst}$ between the tropospheric delay sampled by the DSN antenna and that measured by the calibration instrument at time t is

$$\Delta \tau_{inst}(t) = \sqrt{\left\langle [\tau_{DSN}(\vec{x}_{DSN}, t) - \tau_{cal}(\vec{x}_{DSN} + \vec{\rho}, t)]^2 \right\rangle}$$

$$\qquad (3)$$

where $\vec{\rho}$ is the vector separation in the horizontal plane between the axis of the DSN antenna and the calibration instrument. When delays are averaged over a time Δt (as in a VLBI measurement), the delay difference $\Delta \tau_{avg}$ is

$$\Delta \tau_{avg}(t_0, \Delta t)$$

$$= \frac{1}{\Delta t} \sqrt{\left\langle \left[\begin{array}{c} \int_0^{\Delta t} \tau_{DSN}(\vec{x}_{DSN}, t_0 + t)\, dt \\ \\ - \int_0^{\Delta t} \tau_{cal}(\vec{x}_{DSN} + \vec{\rho}, t_0 + t)\, dt \end{array} \right]^2 \right\rangle} \qquad (4)$$

where t_0 is the epoch at which the integration begins. For all cases in this article where Eqs. (3) and (4) were evaluated, $\theta_{cal} - \theta_{DSN}$ was chosen so as to give a zero mean for the delay difference. Therefore, Eqs. (3) and (4) yielded the standard deviation of the delay difference.

The Allan standard deviation $\sigma_y(\Delta t)$ [6] of the delay difference $\tau_{DSN}(\vec{x}_{DSN}, t) - \tau_{cal}(\vec{x}_{DSN} + \vec{\rho}, t)$ over a time interval Δt is

$$\sigma_y(\Delta t)$$

$$= \sqrt{\frac{\left\langle [\Delta \tau_{inst}(t + 2\Delta t) - 2\Delta \tau_{inst}(t + \Delta t) + \Delta \tau_{inst}(t)]^2 \right\rangle}{2(\Delta t)^2}}$$

$$(5)$$

$\sigma_y(\Delta t)$ will be used as a measure of the delay rate error due to beam mismatch and offset.

B. Method of Calculation

In order to evaluate Eqs. (3)–(5) for given values of d_{DSN}, θ_{DSN}, ϕ_{DSN}, and ψ, the expressions were all expanded to integrals of χ, using Eqs. (1) and (2). Products of integrals were converted to multidimensional integrals, and the order of integration and expectation value was reversed. This resulted in multidimensional integrals of $\langle \chi(\vec{x}_1)\chi(\vec{x}_2) \rangle$, where $\vec{x}_1$ and $\vec{x}_2$ are two different vector locations above the DSN antenna and/or the calibration instrument. These integrals were then converted to integrals of a structure function $D_\chi(\vec{x}_1, \vec{x}_1 - \vec{x}_2)$. $\left(D_\chi(\vec{x}_1, \vec{x}_1 - \vec{x}_2) \equiv \left\langle [\chi(\vec{x}_1) - \chi(\vec{x}_2)]^2 \right\rangle \right)$. This procedure has been described elsewhere [7,5].

The model of [7] was used to evaluate these integrals. This model assumes that time variations in χ are due to spatial variations which move past the observer at a constant vector wind velocity $\vec{v}_w$. It assumes that the wet troposphere has constant average properties up to a height h, with zero refractivity above. D_χ has the analytical form

$$D_\chi(\vec{x}_1, \vec{x}_1 - \vec{x}_2) = \frac{C_\chi^2 R^{2/3}}{1 + (R/L_{sat})^{2/3}} \qquad (6)$$

where $R = \|\vec{x}_1 - \vec{x}_2\|$ and L_{sat} is a saturation length needed to make D_χ converge at large distances. For the calculations reported here, the values of the parameters adopted were $C_\chi = 1.1 \times 10^{-7} \mathrm{m}^{-1/3}$, $L_{sat} = 3000$ km, $v_w = 8$ m/sec, and the slab height $h = 2$ km. These values give the best match to observed 200-sec delay rates and observed daily zenith delay scatter at DSN sites [1]. Connected-element radio interferometric observations over a 20 km-baseline (DSS 13–DSS 15) at Goldstone provide one test of the range over which C_χ can vary.[3] A series of 10 such observations over a period of 2–3 years was analyzed using the model of [7] to fit the observed scatter in residual delays as a function of time separation, angular separation, and elevation angle. One parameter adjustment of C_χ resulted in a χ^2 agreement of approximately 1 per degree of freedom in all cases, with the best-fit value of C_χ always within a factor of 2 of the value used in this article.

The multidimensional integrals of D_χ were evaluated numerically, using Simpson's Rule. The integration step sizes were reduced until convergence was obtained.

C. Validity of Tropospheric Model

Evidence of the validity of this tropospheric model (Kolmogorov turbulence, frozen flow) comes from several arguments. The model prediction for the dependence of delay rate (at a 200-sec time scale) upon elevation angle agrees with the observed shape from 3 years of DSN VLBI data [7]. The phase structure function from non-DSN VLBI observations [8] shows the same power law dependence (with a curvature at integration times near 200 sec) as that predicted by the model. The delay structure function as measured by a solar hygrometer at JPL[4] shows approximately the same power law dependence at short and long time scales as for the model. In addition to the connected-element radio interferometric data (on natural sources) cited above, additional observations of the Ulysses spacecraft with the same interferometer have been performed.[5] When C_χ is adjusted so as to fit point–point delay scatter of adjacent time points, the estimated difference in the zenith delays between the two antennas

---

[3] C. Edwards, personal communication, Tracking Systems and Applications Section, Jet Propulsion Laboratory, Pasadena, California, May 28, 1993.

[4] R. Treuhaft, personal communication, Tracking Systems and Applications Section, Jet Propulsion Laboratory, Pasadena, California, March 1993.

[5] C. Edwards, op. cit.

(DSS 13 and DSS 15) was reproduced within a χ^2 of 1 per degree of freedom.

The tropospheric slab approximation (constant structure function from the surface up to a cutoff altitude) was tested numerically. As described in Section III.A, $\Delta\tau_{inst}$ was calculated for two $(\theta_{DSN}, \phi_{DSN}, \psi)$ cases with a more realistic structure function, one in which the refractivity variations decrease exponentially with height. In these two cases, $\Delta\tau_{inst}$ differed from the slab model value by 3 and 11 percents.

III. Results: Delay Errors

A. Beam Mismatch Effects

This subsection presents the errors which occur when the calibration instrument is mounted on the axis of the DSN antenna. The errors are due to the mismatch between the conical beam of the calibration instrument and the cylindrical beam (a good approximation for the tropospheric volume sampled when observing a point source) of the DSN antenna. For the case where the conical calibration beam, projected to a typical atmospheric height, subtends a much larger diameter than the DSN beam, this error is sometimes referred to as beam smearing. The instantaneous and time-averaged errors are given by Eqs. (3) and (4), respectively, with $\vec{\rho} = 0$ in both cases.

1. Zero Integration Time (Instantaneous Beam Mismatch Error). The simplest approximation used was a pencil DSN beam (i.e., a cylinder of diameter zero), a conical calibration beam, and zero integration time. Results are shown in Fig. 1. Note that $\theta_{cal} - \theta_{DSN} > 0$ in order to remove the systematic offset between τ_{cal} and τ_{DSN}.

Seven of the values shown in Fig. 1 were recalculated, using a 34-m-diam DSN antenna beam. The physical mismatch between such a beam and a conical calibration beam was smaller than for a pencil DSN beam. When the maximum calibration-beam diameter $(\psi h/\sin\theta_{DSN})$ was not substantially larger than the DSN beam diameter (h is the wet troposphere slab height), there was a significant reduction in the delay calibration error $\Delta\tau$. (For these cases, the DSN cylindrical beam is a significantly better match to the conical calibration beam than is a pencil beam.) However, these were the cases where the delay error was small (<0.1 mm) with a pencil beam calculation. When a pencil beam calculation yielded a delay error >0.1 mm, the delay error with a cylindrical DSN beam was only slightly smaller than with a pencil DSN beam.

For instantaneous ($\Delta t = 0$) results, no transport of refractivity irregularities occurs. The results represent purely spatial irregularities and do not depend on the wind velocity or direction.

2. Nonzero Integration Time. For four cases, the beam mismatch error was calculated for integration times of 10 and 100 sec, with a 34-m-diam DSN beam. For nonzero integration times, some of the refractivity irregularities move through both beams, reducing the beam mismatch error. A wind velocity of 8 m/sec was assumed, with an azimuth 45 deg different from the DSN pointing direction (the dependence of the time-averaged error upon wind direction was not tested, due to limited computer time). The results are shown in Fig. 2. Delay integration for 100 sec reduces the beam mismatch error by factors of 1.2–2.2. The smaller factors correspond to cases where the instantaneous beam mismatch error was largest. For these cases, the DSN beam cross-sectional area at most heights is much smaller than that of the calibration beam. Therefore, most of the refractivity irregularities in the calibration beam which are transported by the wind are never seen by the DSN beam, and time averaging has little effect.

For an overall line-of-sight calibration accuracy goal of 1 mm, it is desirable that any one error component contribute no more than 20 percent to a 1-mm^2 total variance. This yields a maximum allowed beam-mismatch error of $\sqrt{0.20}$ mm = 0.45 mm. For a 100-sec integration time, a 1-deg full-width calibration beam is acceptable at all elevation angles, and a 2-deg full-width beam is acceptable for elevation angles larger than approximately 7–8 deg.

3. Test of Wet Troposphere Slab Approximation. As a test of the validity of the wet troposphere slab model, the instantaneous delay error with a pencil DSN beam was recalculated using a modified structure function for two sets of (θ_{DSN}, ψ) parameters. This structure function was adopted from previous work[6] and had the form

$$D_\chi(\vec{x}_1, \vec{x}_1 - \vec{x}_2) = \frac{C_\chi^2 R^{2/3}}{1 + (R/L_{sat})^{2/3}} e^{-(z_1 + z_2)/z_0} \quad (7)$$

where $R = \|\vec{x}_1 - \vec{x}_2\|$, z_1 and z_2 are the heights of the two points $\vec{x}_1$ and $\vec{x}_2$, L_{sat} is a saturation scale length, and z_0 is a wet troposphere scale height. This structure function accounts for the falloff of water vapor density with height.

[6] J. J. Wiseman, "Altitude Dependence and Saturation Modifications to the Treuhaft-Lanyi Model of Tropospheric Delay Fluctuations," JPL Interoffice Memorandum 335.3–87–203 (internal document), Jet Propulsion Laboratory, Pasadena, California, December 21, 1987.

Values of $C_\chi = 1.34 \times 10^{-7} \mathrm{m}^{-1/3}$, $L_{sat} = 3000$ km, and $z_0 = 2$ km were used.[7] The upper height of integration was 10 km. The results (for zero integration time and a pencil, or zero-diameter, DSN beam) were 0.15 mm for $\theta_{DSN} = 10$ deg and $\psi = 1$ deg, and 0.066 mm for $\theta_{DSN} = 30$ deg and $\psi = 2$ deg. These results differed from the corresponding values in a slab model by 11 and 3 percents, respectively. This level of agreement suggests that the use of a wet troposphere slab approximation was a reasonable one for the purpose of calculating beam mismatch errors.

4. Application to Beams With Tapered Gain Profiles. The beam mismatch results presented in Figs. 1 and 2 are for a uniform calibration beam gain out to a sharp cutoff at $\psi/2$. Actual beam profiles will be tapered, with a Gaussian profile often used for analytical calculations. A Gaussian profile was not used for the calculations in this article because it would have required an excessive amount of computer time.

An approximate correspondence between Gaussian HPBW and the full width ψ of a uniform gain beam profile used in these calculations can be made. In Fig. 1, the dependence of the beam mismatch error $\Delta\tau_{inst}$ upon beamwidth ψ is $\Delta\tau_{inst} \propto \psi^{exp}$, where $exp \approx 1$ at low elevation angles ($\theta_{DSN} = 6$ or 10 deg) where the error is of most concern (i.e., largest). For a circular beam with a uniform gain out to a sharp cutoff, the mean value $\bar\xi_{uniform}$ for the angular separation from the axis is $\bar\xi_{uniform} = \psi/3$. For a circular beam with a Gaussian profile, the mean value $\bar\xi_{Gaussian}$ for this separation is $\bar\xi_{Gaussian} = \mathrm{HPBW}\sqrt{\pi}/4\sqrt{\ln 2} \approx 0.532\ \mathrm{HPBW}$. Assume that $\Delta\tau_{inst} \propto \psi^{exp} \implies \Delta\tau_{inst} \propto \bar\xi^{exp}$. For $\Delta\tau_{inst}(uniform) = \Delta\tau_{inst}(Gaussian), \bar\xi_{uniform} = \bar\xi_{Gaussian}$, which yields $\mathrm{HPBW} = 0.63\psi$. Therefore, beam mismatch errors in Figs. 1 and 2 will apply approximately to $\mathrm{HPBW} = 0.63\psi$. A roughly similar relation will hold for beam-mismatch delay rates (Tables 1–2, discussed in Section IV.B). For both delay and delay rate, the correspondence factor will differ very little from 0.63 at higher elevation angles (e.g., the factor is 0.64 if $\Delta\tau_{inst} \propto \psi^{0.8}$, as observed at $\theta_{DSN} = 60$ deg for delay errors).

5. Tests of Numerical Computations. The accuracy of the numerical integrations used to generate the beam mismatch results was tested in two ways. The first test used a quadratic structure function.

$$D_\chi(R) = C_\chi^2 R^2 \qquad (8)$$

Using this structure function, the integrals could be evaluated analytically in many cases [8] (e.g., with pencil DSN or calibration beams, cylindrical DSN beams, or fan calibration beams: a nonzero angular extent in only one dimension). The analytical and numerical beam mismatch results for the quadratic structure function agreed to seven significant figures.

The second test consisted of independent numerical integrations, using the structure function of Eq. (6). These calculations used a code written for the formalism in [5], corrected for a numerical error [9]. A diverging beam with a square cross section and uniform gain was used in these calculations. For a square beam, $\bar\xi_{uniform}(square\ beam) = 0.383\psi = 1.15\bar\xi_{uniform}(circular\ beam)$. Given the assumed relationship between $\Delta\tau_{inst}$ and $\bar\xi$ discussed above, one would expect $\Delta\tau_{inst}(square\ beam) \approx 1.15\Delta\tau_{inst}(circular\ beam)$ for the same value of ψ. For the seven (θ_{DSN}, ψ) cases that were checked, the ratio $\Delta\tau_{inst}(square\ beam) : \Delta\tau_{inst}(circular\ beam)$ was in the range 1.06–1.27, with a mean value of 1.15.

B. Beam Offset Effects

1. Results for Nonzero Integration Time. For a nonzero DSN-calibration beam offset [i.e., $\vec\rho \neq 0$ in Eqs. (3) and (4)], the number of parameters (beamwidth, elevation angle, DSN-calibration offset distance and azimuth, and wind velocity and azimuth) becomes large. A simplified calculation was necessary in order to explore a reasonable volume of parameter space with the available computer resources. A pencil beam (zero diameter) was used for both the DSN antenna beam and the calibration beam. For this case, $\theta_{cal} = \theta_{DSN}$ gives a delay difference with zero mean.

For a given vector separation $\vec\rho$, the offset error depends on two azimuths: that of $\vec\rho$ and that of $\vec v_w$ (in both cases, it is the azimuth relative to the DSN pointing direction which is important). Using pencil beams, the beam offset error was calculated for all combinations of these two azimuths (with grid spacings of 30 deg). Figures 3–5 show the results for separations ($\|\vec\rho\|$) of 17, 50, and 100 m, and integration times of 30, 60, 120, and 240 sec. Figure 3 gives results for an elevation angle of 60 deg, Fig. 4 for an elevation angle of 20 deg, and Fig. 5 for an elevation angle of 6 deg. The lowest elevation angle currently used by the DSN for spacecraft tracking is 6 deg. The error bars in Figs. 3–5 represent the standard deviation for the 144 azimuth pairs for each separation distance ρ and integration time.

---

[7] Ibid.

[8] G. Lanyi, personal communication, Tracking Systems and Applications Section, Jet Propulsion Laboratory, Pasadena, California, 1992.

For a 60-sec integration time and a maximum allowed error of 0.45 mm (i.e., a 20-percent contribution to a 1-mm^2 total variance), a separation of 50 m is acceptable at all elevation angles, and a separation of 100 m is acceptable at elevation angles larger than 15 deg.

2. Tests of Numerical Results. In order to check the validity of the use of pencil beams for these calculations, two cases were recalculated using more realistic beams (i.e., a 34-m-diam cylindrical DSN beam and a conical calibration beam). Both cases used $\theta_{DSN} = 10$ deg, $\psi = 1$ deg, an integration time of 100 sec, and a wind velocity of 8 m/sec in azimuth 45 deg. Case 1 had a 17-m DSN-calibration instrument separation in azimuth 90 deg, and case 2 had a 50-m separation in azimuth 0 deg. All azimuths are relative to the DSN pointing direction. The results agreed with the quadrature sum of the beam mismatch (i.e., the zero separation error) and the pencil-beam offset error to within 2 percent in both cases.

The pencil beam results for a limited number of cases (16 combinations of elevation angle, separation distance and azimuth, wind azimuth, and integration time) were recalculated, using a different analytical derivation and computer code. In all 16 cases, the time-averaged beam offset error calculations agreed to <2 percent.

IV. Results: Delay Rate Errors

A. Beam Mismatch Effects

The beam mismatch errors for delay rates [expressed as an Allan standard deviation: Eqs. (3) and (5) with $\vec{p} = 0$] were calculated for a cylindrical 34-m-diam DSN beam and a conical calibration beam as a function of elevation angle θ_{DSN}, calibration beam full width ψ, and time interval Δt. Results are given in Table 1 ($\theta_{DSN} = 60$ deg) and Table 2 ($\theta_{DSN} = 20$ deg). The values of $\psi = 1$ deg and $\psi = 2$ deg from Table 2 are plotted in Fig. 6. An elevation angle of 20 deg is the lowest currently used for spacecraft Doppler tracking for navigation purposes, and is the lowest planned for use during the Cassini Gravitational Wave experiment. Column 6 in Tables 1 and 2 gives the Allan standard deviation of the uncalibrated wet troposphere for purposes of comparison. (It was calculated for a 34-m-diam cylindrical beam pointed in a constant direction at that elevation angle). The results in Tables 1 and 2 are averages over wind azimuth with a grid of 30 deg. The variation with wind direction was <5 percent for all cases except for the 10-sec values at 20-deg elevation, where the 1σ variation ranged from 5 percent at $\psi = 0.5$ deg to 38 percent at $\psi = 4$ deg. In addition, the 1σ variation for $\Delta t = 32$ sec, $\psi = 4$ deg, and $\theta_{DSN} = 20$ deg was 9 percent.

For short time scales, other known error sources will dominate over the beam mismatch error for small beamwidths. Projected state-of-the-art frequency-standard capability for the year 2000[9] is an Allan standard deviation of 1×10^{-15} for $\Delta t = 1$–100 sec from a superconducting cavity maser oscillator and $1 \times 10^{-14}/\sqrt{\Delta t}$ for $\Delta t = 100$–10,000 sec from a trapped-ion frequency standard. If water vapor radiometers are used for troposphere calibration (as seems likely), thermal receiver noise will be significant on short time scales. A WVR with a 200-MHz bandwidth and a 300-K total on-sky system temperature, operated in a total power mode, will give an Allan standard deviation of $7.4 \times 10^{-13}(\Delta t)^{-1}t_{integ}^{-0.5}$, where t_{integ} is the WVR integration time (in seconds) used for calibration. In Table 3, the quadrature sums of the Allan standard deviations for beam mismatch error, frequency standard noise, and WVR receiver noise (using the above parameters for the WVR and frequency standard) are given for an elevation angle of 30 deg and beamwidths of 0.5, 1, 2, and 4 deg. The assumed WVR integration time was $t_{integ} = 10$ sec for $\Delta t < 100$ sec, and $t_{integ} = 100$ sec for $\Delta t \geq 100$ sec. The improvement with decreasing beamwidth is substantial down to ψ of approximately 1 deg for timescales up to $\Delta t = 1000$ sec. The improvement is weak for $\psi < 1$ deg and $\Delta t > 1000$ sec. If future frequency standards do not achieve the performance goals given above, delay-rate troposphere calibration will be limited by the frequency standards over a larger range of parameter space (e.g., for time scales shorter than 1000 sec and beamwidths wider than $\psi = 1$ deg).

B. Beam Offset Effects

The delay-rate beam offset errors were calculated [Eqs. (3) and (5) with $\vec{p} \neq 0$] for offsets of 17, 50, and 100 m, using full beamwidths (ψ) of 0.5, 1, 2, and 4 deg. The resulting Allan standard deviations were averaged over all wind directions (with a 30-deg grid) and over two DSN-calibration separation azimuths: 0 and 90 deg (as before, all azimuths are relative to the DSN pointing direction). Results (mean and standard deviation) are given in Tables 4 ($\theta_{DSN} = 60$ deg) and 5 ($\theta_{DSN} = 20$ deg). The 17-, 50-, and 100-m values from Table 5 are plotted in Fig. 7. Note that, for a 100-m offset, the beam offset error exceeds the uncalibrated troposphere for time scales less than approximately the crossing time by the wind (100 m/8 m/sec = 12.5 sec). For longer time scales, the offset error decreases, due to the transport of refractivity irregularities. Tables 4 and 5 list results for only one beamwidth: $\psi = 1$ deg. Calculations for other beamwidths indicate a

---

[9] G. J. Dick, personal communication, Communications Systems Research Section, Jet Propulsion Laboratory, Pasadena, California, January 27, 1993.

weak dependence (<5 percent) upon beamwidth for separations $\rho \geq 50$ m. For $\rho = 17$ m, the mean Allan standard deviations varied by approximately ± 10 percent with beamwidth at a 60-deg elevation angle. At $\rho = 17$ m and $\theta_{DSN} = 20$ deg, the mean Allan standard deviations for $\psi = 0.5, 2,$ and 4 deg are approximately 0.85, 1.5, and 2.5 times that at $\psi = 1$ deg.

A DSN-calibration instrument offset has a severe impact on the accuracy of delay rate calibration. For a 50-m separation, which is probably near the minimum for a location off the antenna, the goals of the Cassini Gravitational Wave Search experiment cannot be met at time scales less than 3000–4000 sec, and the requirements cannot be met at time scales less than 500 sec. The use of multiple troposphere calibration instruments could potentially reduce the error. Due to time variation in wind azimuth, at least three instruments arrayed around the perimeter of a DSN antenna would be needed in order to achieve a significant reduction in the offset error.

V. Discussion

The consequences of a beam mismatch and offset between a DSN antenna and a calibration instrument (e.g., a WVR) are much more serious for delay rate measurements than for time-averaged delay measurements. This situation reflects the fact that differentiating a noisy signal (the wet tropospheric refractivity in this case) increases its amplitude, whereas integrating such a signal decreases its amplitude. For delay measurements with ≥ 1-min integration, HPBW ≤ 1.3 deg and an offset ≤ 50 m are needed for an overall calibration goal of 1 mm. A narrower beamwidth and an on-axis location would be desirable, in case other error sources should prove to be small enough to achieve a calibration accuracy of <1 mm.

For delay rate measurements, the performance cost of an offset location for a calibration instrument is severe. A calibration instrument that could measure line-of-sight delay perfectly, but which had a 50-m offset from the axis of a DSN antenna, would calibrate only 96 percent of the total 1000-sec troposphere Allan standard deviation, 80 percent for 100-sec intervals, and could do no useful calibration for 10-sec time scales (these values are for a 20-deg elevation angle; the fractional calibration errors are approximately a factor of 2 smaller at 60 deg). *An on-axis location for a calibration instrument is essential in order to perform accurate tropospheric delay rate measurements.* Specifically, it is required in order to meet the Cassini Gravitational Wave Search *goals* at time scales less than 3000–4000 sec, or the *requirements* at times scales less than 500 sec. Multiple calibration instruments mounted around the perimeter of the DSN antenna could potentially reduce the offset error, but this has not been quantified. Given the high cost of water-vapor-sensing instruments (e.g., WVR's), this is not an attractive option.

A calculation of the power spectral density error resulting from an offset location reached conclusions similar to the results shown in Tables 4 and 5.[10] That power spectral density calculation was done in a very different manner from the calculations reported here (although it used the same wet troposphere fluctuation model [7]).

The beam mismatch error (i.e., that for zero on-axis offset) is important for time scales of 1000 sec and smaller. This error drops rapidly as the beamwidth is reduced, down to HPBW = 0.7 deg. The improvement for HPBW <0.7 deg is minor, due to contributions from other error sources (frequency standard noise and WVR thermal receiver noise). For HPBW = 0.7 deg, the beam mismatch error will not interfere with the Cassini Gravitational Wave Search *requirements* at any time scale. It will prevent the *goals* from being met at time scales shorter than 200 sec.

---

[10] P. Richter, personal communication, Telecommunications Systems Section, Jet Propulsion Laboratory, Pasadena, California, 1993.

References

[1] R. N. Treuhaft and S. T. Lowe, "A Measurement of Planetary Relativistic Deflection," *The Astronomical Journal*, vol. 102, no. 5, pp. 1879–1888, November 1991.

[2] G. Elgered, J. L. Davis, T. A. Herring, and I. I. Shapiro, "Geodesy by Radio Interferometry: Water Vapor Radiometry for Estimation of the Wet Delay," *Journal of Geophysical Research*, vol. 96, no. B4, pp. 6541–6555, April 10, 1991.

[3] W. L. Smith, H. E. Revercomb, H. B. Howell, H.-L. Huang, R. O. Knuteson, E. W. Koenig, D. D. LaPorte, S. Silverman, L. A. Sromovsky, and II. M. Woolf, "GHIS—The GOES High-Resolution Interferometer Sounder," *Journal of Applied Meteorology*, vol. 29, pp. 1189–1204, December 1990.

[4] D. M. Tralli, S. M. Lichten, and T. A. Herring, "Comparison of Kalman Filter Estimates of Zenith Atmospheric Path Delays Using the Global Positioning System and Very Long Baseline Interferometry," *Radio Science*, vol. 27, no. 6, pp. 999–1007, November–December 1992.

[5] J. Z. Wilcox, "The Effect of Tropospheric Fluctuations on the Accuracy of Water Vapor Radiometry," *The Telecommunications and Data Acquisition Progress Report 42-110*, vol. April–June 1992, Jet Propulsion Laboratory, Pasadena, California, pp. 33–51, August 15, 1992.

[6] D. W. Allan, "Statistics of Atomic Frequency Standards," *Proceedings of the IEEE*, vol. 54, no. 2, pp. 221–230, February 1966.

[7] R. N. Treuhaft and G. E. Lanyi, "The Effect of the Dynamic Wet Troposphere on Radio Interferometric Measurements," *Radio Science*, vol. 22, no. 2, pp. 251–265, March–April 1987.

[8] A. E. E. Rogers, "Coherence Limits in VLBI Observations at 3-millimeter Wavelength," *Radio Science*, vol. 19, no. 6, pp. 1552–1560, November–December 1984.

[9] J. Z. Wilcox, "Errata: The Effect of Tropospheric Fluctuations on the Accuracy of Water Vapor Radiometry," *The Telecommunications and Data Acquisition Progress Report 42-114*, vol. April–June 1993, Jet Propulsion Laboratory, Pasadena, California, p. 346, August 15, 1993.

Table 1. Beam mismatch Allan standard deviation between a conical calibration beam and a coaxial 34-m-diam DSN beam for a 60-deg elevation angle.

Time interval (Δt), sec	Full beamwidth (ψ), deg				Uncalibrated troposphere, Allan standard deviation
	0.5	1	2	4	
10	1.0×10^{-14}	7.8×10^{-15}	1.1×10^{-14}	2.6×10^{-14}	6.4×10^{-14}
32	3.2×10^{-15}	2.4×10^{-15}	3.5×10^{-15}	8.0×10^{-15}	5.5×10^{-14}
100	1.0×10^{-15}	7.7×10^{-16}	1.1×10^{-15}	2.6×10^{-15}	4.3×10^{-14}
320	3.2×10^{-16}	2.4×10^{-16}	3.5×10^{-16}	8.0×10^{-16}	2.9×10^{-14}
1000	1.0×10^{-16}	7.7×10^{-17}	1.1×10^{-16}	2.6×10^{-16}	1.6×10^{-14}
3200	3.2×10^{-17}	2.4×10^{-17}	3.5×10^{-17}	8.0×10^{-17}	8.0×10^{-15}
10,000	1.0×10^{-17}	7.7×10^{-18}	1.1×10^{-17}	2.6×10^{-17}	3.8×10^{-15}

Table 2. Beam mismatch Allan standard deviation between a conical calibration beam and a coaxial 34-m-diam DSN beam for a 20-deg elevation angle.

Time interval (Δt), sec	Full beamwidth (ψ), deg				Uncalibrated troposphere, Allan standard deviation
	0.5	1	2	4	
10	1.3×10^{-14}	2.2×10^{-14}	4.3×10^{-14}	5.9×10^{-14}	8.3×10^{-14}
32	4.3×10^{-15}	7.4×10^{-15}	1.7×10^{-14}	3.2×10^{-14}	7.5×10^{-14}
100	1.3×10^{-15}	2.4×10^{-15}	5.6×10^{-15}	1.1×10^{-14}	6.3×10^{-14}
320	4.2×10^{-16}	7.4×10^{-16}	1.7×10^{-15}	3.5×10^{-15}	5.1×10^{-14}
1000	1.3×10^{-16}	2.4×10^{-16}	5.6×10^{-16}	1.1×10^{-15}	3.5×10^{-14}
3200	4.1×10^{-17}	7.3×10^{-17}	1.7×10^{-16}	3.5×10^{-16}	1.9×10^{-14}
10,000	1.3×10^{-17}	2.4×10^{-17}	5.6×10^{-17}	1.1×10^{-16}	9.3×10^{-15}

Table 3. Total Allan standard deviation due to beam mismatch, frequency standard noise, and WVR receiver noise for a 30-deg elevation angle and an on-axis location.

Time interval (Δt), sec	Full beamwidth (ψ), deg			
	0.5	1	2	4
10	2.6×10^{-14}	2.7×10^{-14}	3.7×10^{-14}	5.4×10^{-14}
32	8.0×10^{-15}	8.4×10^{-15}	1.2×10^{-14}	2.0×10^{-14}
100	1.7×10^{-15}	1.9×10^{-15}	3.2×10^{-15}	6.3×10^{-15}
320	7.0×10^{-16}	7.4×10^{-16}	1.1×10^{-15}	2.0×10^{-15}
1000	3.5×10^{-16}	3.6×10^{-16}	4.4×10^{-16}	7.0×10^{-16}
3200	1.8×10^{-16}	1.9×10^{-16}	2.0×10^{-16}	2.6×10^{-16}
10,000	1.0×10^{-16}	1.0×10^{-16}	1.0×10^{-16}	1.2×10^{-16}

Table 4. Allan standard deviation for an offset between a conical calibration beam and a 34-m-diam DSN beam for a 60-deg elevation angle and a 1-deg full beamwidth.

Time interval (Δt), sec	DSN-calibration separation, m			Uncalibrated troposphere, Allan standard deviation
	17	50	100	
10	$3.0 \pm 0.4 \times 10^{-14}$	$7.1 \pm 1.0 \times 10^{-14}$	$9.2 \pm 1.3 \times 10^{-14}$	6.4×10^{-14}
32	$1.1 \pm 0.1 \times 10^{-14}$	$2.8 \pm 0.2 \times 10^{-14}$	$4.6 \pm 0.5 \times 10^{-14}$	5.5×10^{-14}
100	$3.8 \pm 0.3 \times 10^{-15}$	$1.0 \pm 0.1 \times 10^{-14}$	$1.7 \pm 0.1 \times 10^{-14}$	4.3×10^{-14}
320	$1.2 \pm 0.1 \times 10^{-15}$	$3.2 \pm 0.2 \times 10^{-15}$	$5.6 \pm 0.2 \times 10^{-15}$	2.9×10^{-14}
1000	$4.0 \pm 0.2 \times 10^{-16}$	$1.0 \pm 0.1 \times 10^{-15}$	$1.8 \pm 0.1 \times 10^{-15}$	1.6×10^{-14}
3200	$1.2 \pm 0.1 \times 10^{-16}$	$3.2 \pm 0.2 \times 10^{-16}$	$5.6 \pm 0.2 \times 10^{-16}$	8.0×10^{-15}
10,000	$4.0 \pm 0.2 \times 10^{-17}$	$1.0 \pm 0.1 \times 10^{-16}$	$1.8 \pm 0.1 \times 10^{-16}$	3.8×10^{-15}

Table 5. Allan standard deviation for an offset between a conical calibration beam and a 34-m-diam DSN beam for a 20-deg elevation angle and a 1-deg full beamwidth.

| Time interval (Δt), sec	DSN-calibration separation, m			Uncalibrated troposphere, Allan standard deviation
	17	50	100	
10	$3.4 \pm 1.8 \times 10^{-14}$	$7.1 \pm 4.1 \times 10^{-14}$	$9.4 \pm 4.4 \times 10^{-14}$	8.3×10^{-14}
32	$1.3 \pm 0.6 \times 10^{-14}$	$3.6 \pm 1.5 \times 10^{-14}$	$5.2 \pm 2.3 \times 10^{-14}$	7.5×10^{-14}
100	$4.8 \pm 2.1 \times 10^{-15}$	$1.2 \pm 0.5 \times 10^{-14}$	$2.0 \pm 0.8 \times 10^{-14}$	6.3×10^{-14}
320	$1.6 \pm 0.6 \times 10^{-15}$	$4.0 \pm 1.6 \times 10^{-15}$	$7.2 \pm 2.6 \times 10^{-15}$	5.1×10^{-14}
1000	$5.2 \pm 2.0 \times 10^{-16}$	$1.3 \pm 0.5 \times 10^{-15}$	$2.4 \pm 0.8 \times 10^{-15}$	3.5×10^{-14}
3200	$1.6 \pm 0.6 \times 10^{-16}$	$4.0 \pm 1.6 \times 10^{-16}$	$7.2 \pm 2.6 \times 10^{-16}$	1.9×10^{-14}
10,000	$5.2 \pm 2.0 \times 10^{-17}$	$1.3 \pm 0.5 \times 10^{-16}$	$2.4 \pm 0.8 \times 10^{-16}$	9.3×10^{-15}
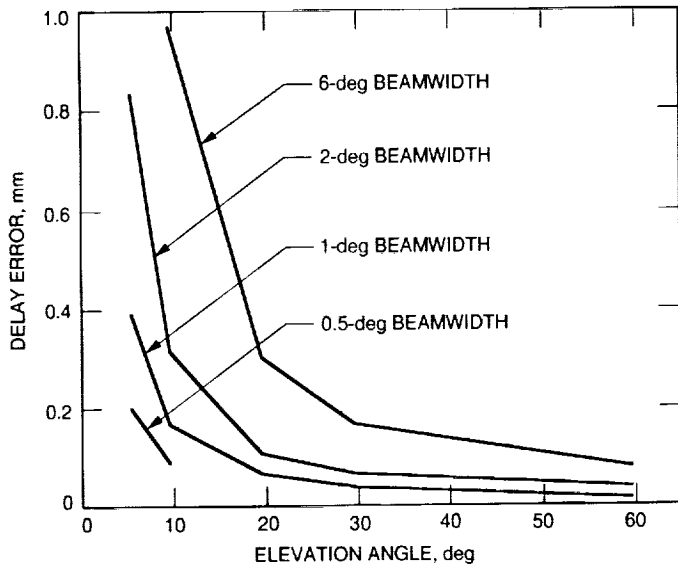
Fig. 1. Instantaneous delay calibration error due to beam mismatch as a function of elevation angle (θ) and full beamwidth (ψ) (circular beamwidth with a uniform gain) for a pencil DSN beam.
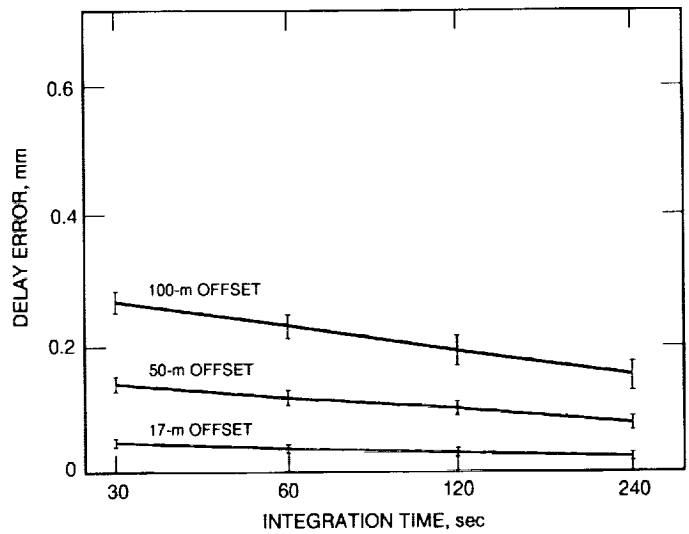

Fig. 3. Time-averaged delay calibration error due to beam offset as a function of time for offsets (between the axis of the DSN antenna and the calibration instrument) of 17, 50, and 100 m. The elevation angle is 60 deg. A pencil DSN beam was used in the calculations.
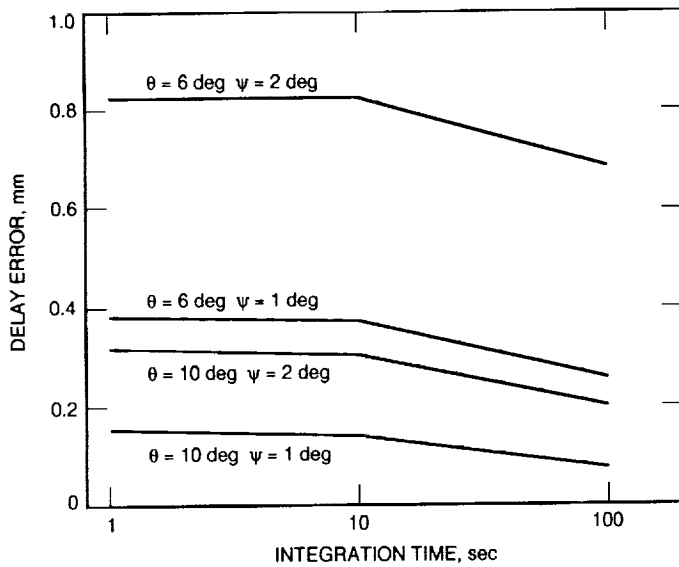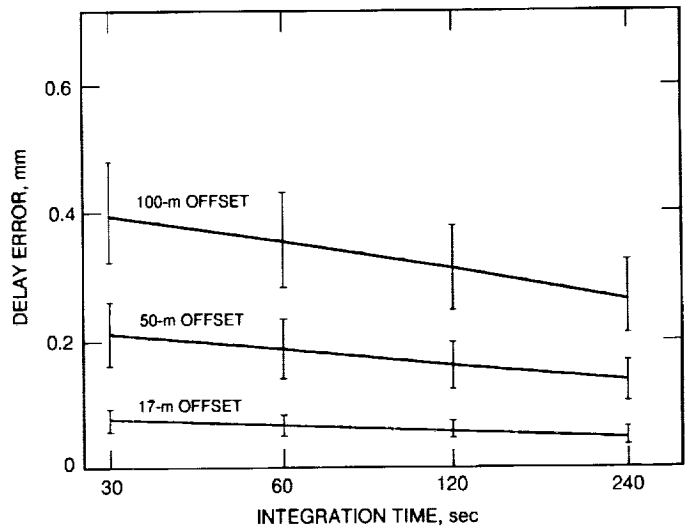

Fig. 2. Time-averaged delay calibration error due to beam mismatch for four combinations of elevation angle (θ) and full beamwidth (ψ) (circular beam with a uniform gain). A 34-m diam DSN beam was used in the calculations.

Fig. 4. Time-averaged delay calibration error due to beam offset as a function of time for offsets (between the axis of the DSN antenna and the calibration instrument) of 17, 50, and 100 m. The elevation angle is 20 deg. A pencil DSN beam was used in the calculations.
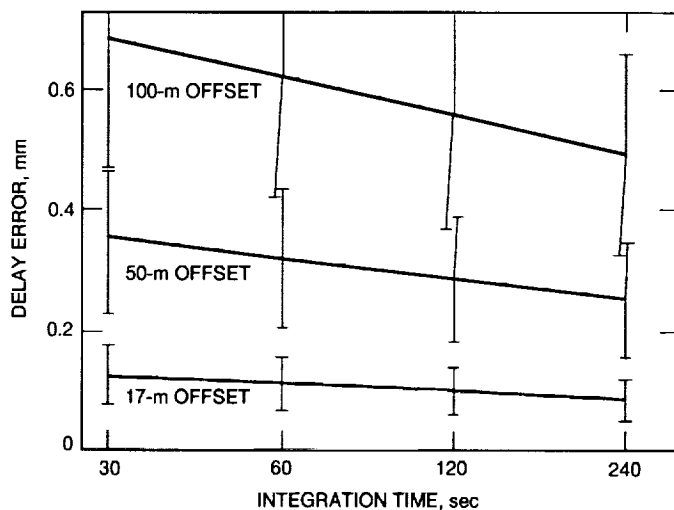
Fig. 5. Time-averaged delay calibration error due to beam offset as a function of time for offsets (between the axis of the DSN antenna and the calibration instrument) of 17, 50, and 100 m. The elevation angle is 6 deg. A pencil DSN beam was used in the calculations.
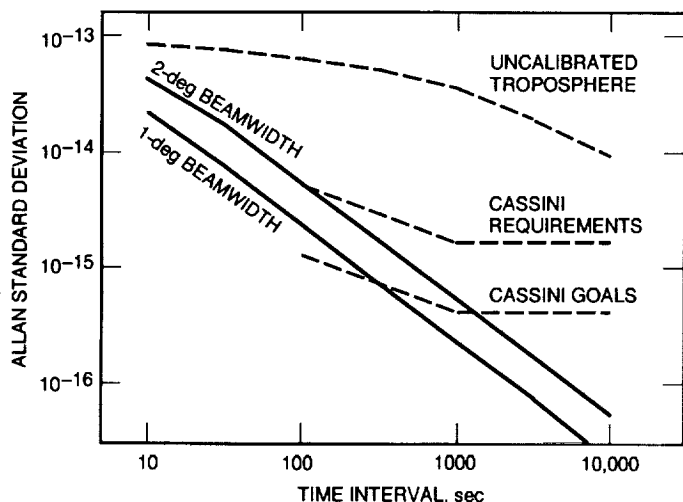

Fig. 6. Delay rate calibration error (expressed as an Allan standard deviation) due to beam mismatch as a function of time interval for full beamwidths ψ (circular beam with a uniform gain) of ψ = 2 deg and ψ = 1 deg. The elevation angle is 20 deg. The Allan standard deviation of the uncalibrated troposphere is plotted for comparison, as are the goals and requirements of the Cassini Gravitational Wave Search experiment. A 34-m-diameter DSN beam was used in the calculations.
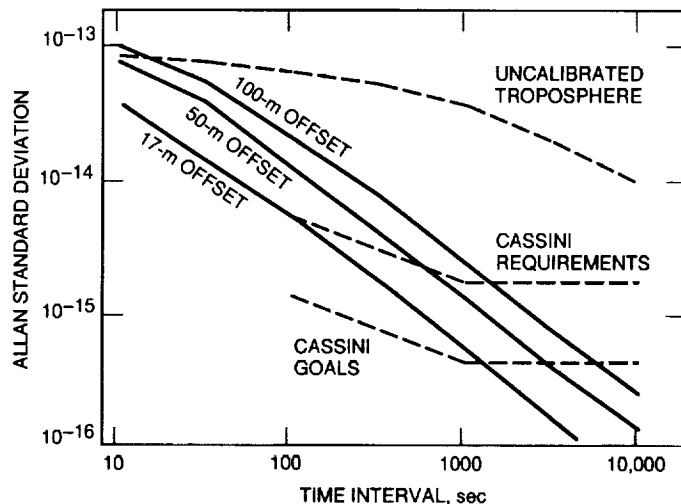

Fig. 7. Delay rate calibration error (expressed as an Allan standard deviation) due to beam offset as a function of time interval for offsets (between the axis of the DSN antenna and the calibration instrument) of 17, 50, and 100 m. The elevation angle is 20 deg. The Allan standard deviation of the uncalibrated troposphere is plotted for comparison, as are the goals and requirements of the Cassini Gravitational Wave Search experiment. A 34-m-diameter DSN beam was used in the calculations.